Polymer 258 (2022) 125316

Contents lists available at ScienceDirect

Polymer

journal homepage: www.elsevier.com/locate/polymer

Cross-evaluation of stiffness measurement methods for hydrogels

Nathan R. Richbourg [a], Manuel K. Rausch [a,b,c], Nicholas A. Peppas [a,d,e,f,*]

[a] Department of Biomedical Engineering, University of Texas, Austin, TX, 78712, USA
[b] Department of Aerospace Engineering & Engineering Mechanics, University of Texas, Austin, TX, 8712, USA
[c] Oden Institute for Computational Engineering & Sciences, University of Texas, Austin, TX, 78712, USA
[d] McKetta Department of Chemical Engineering, University of Texas, Austin, TX, 78712, USA
[e] Division of Molecular Therapeutics and Drug Delivery, College of Pharmacy, University of Texas, Austin, TX, 78712, USA
[f] Departments of Surgery and Pediatrics, Dell Medical School, University of Texas, Austin, TX, 78712, USA

ARTICLE INFO

Keywords:
Hydrogel
Stiffness
Rubberlike elasticity
Hyperelastic model
Swollen polymer network

ABSTRACT

Stiffness is a key property for hydrogels, affecting cellular adhesion, motility, and differentiation, the integrity of biomedical implants, and the flexibility of wound coverings. A hydrogel's stiffness is controlled by its synthesis conditions, whether by changing the polymer or crosslinking scheme used, increasing the concentration of polymer, or increasing the extent of crosslinking. However, no universal design scheme for controlling hydrogel stiffnesses has been previously proposed, and comparisons between different studies are limited by inconsistent measurement methods. Here, we used a structural model to make *a priori* predictions of the stiffness of eighteen poly(vinyl alcohol) hydrogel formulations and compared five independent stiffness measurement methods to establish broadly applicable standards for predicting and measuring the stiffness of hydrogels. Overall stiffness differences between the five measurement methods (tension, compression, shear rheology, macroindentation, and nanoindentation) were small, but each method provided distinct insights, including measurements of Poisson's ratio and viscoelasticity. The measured hydrogel stiffnesses increased with increasing initial polymer volume fractions (φ_0) and decreased with increasing degrees of polymerization between junctions (N_j), matching fundamental predictions. Strong correlations between swelling and stiffness in hydrogels suggested a mechanism for improving the accuracy of the predictive model. These results suggest that our predictive model is a powerful tool for the rational design of hydrogels with desirable stiffnesses for a variety of biomedical applications.

1. Introduction

Water-swollen polymer networks, or hydrogels, are a highly studied group of materials, largely valued for their use in biomedical applications such as soft tissue-mimicking scaffolds [1], drug delivery reservoirs [2], and biocompatible coatings for devices such as stents and wound wrappings [3]. For nearly all biomedical applications of hydrogels, their stiffness is a critical design parameter [4]. When hydrogels are used as 2D substrates and 3D environments for cell culture, their stiffness affects cell motility [5,6] and can initiate signaling cascades that drive stem cell differentiation along specific pathways [7,8]. For hydrogel implants, including slow-releasing drug reservoirs, matching the surrounding environment's stiffness reduces differential stress applied to the implant that can dislocate, degrade, or fibrotically isolate the implant [9]. Similarly, hydrogel coatings for biomedical devices must exhibit flexibility and adhesion to the underlying material with interactions with the surrounding or contained biological components, which may also introduce shear stresses, such as by blood flowing through a hydrogel-coated stent [10,11]. For these and many more cases, a hydrogel's stiffness must be tuned precisely and reliably over the broad range of stiffnesses found in the human body.

Creating consistent models for controlling hydrogel stiffness requires several assumptions about hydrogel structure and the definition of stiffness [12,13]. Here, we specifically address equilibrium-swollen hydrogels with stable network structures created by irreversible covalent crosslinking reactions. While this classification does not apply to all hydrogels, it provides a foundation relevant to many hydrogel formulations and facilitates practical investigation into how the structural features of such stable hydrogels contribute to their stiffness. We also adopt an incompressible, neo-Hookean hyperelastic model [14,15], which simplifies the definition of stiffness into the single shear modulus parameter relating stress and strain. Notably, the hyperelastic modeling

* Corresponding author. . Department of Biomedical Engineering, University of Texas, Austin, TX, 78712, USA.
E-mail address: peppas@che.utexas.edu (N.A. Peppas).

https://doi.org/10.1016/j.polymer.2022.125316
Received 31 March 2022; Received in revised form 28 July 2022; Accepted 7 September 2022
Available online 11 September 2022

approach does not account for viscoelastic [16] and poroelastic phenomena [17–19], instead treating the hydrogel as perfectly elastic. Moreover, the neo-Hookean model specifically limits the material description to be isotropic. This is a dramatic oversimplification of hydrogel properties and cannot be justified at large deformations or especially long or short timescales, but it ultimately serves the same purpose as the hydrogel structural assumptions, to facilitate the investigation of foundational structure-stiffness relationships that can then be extended with careful modifications to the study of more complex systems and conditions.

Our understanding of how hydrogel structure affects stiffness extends from rubberlike elasticity theory, which includes mathematical models relating hydrogel structural parameters to stiffness [12,20]. Specifically, our recent efforts to update the swollen polymer network model provide an approach for *a priori* prediction of a specific hydrogel formulation's shear modulus based on synthesis-defined structural parameters [12,21]. Notably, the swollen polymer network model and the neo-Hookean hyperelastic model are compatible, both summarizing stiffness as the shear modulus and including assumptions of elasticity and incompressibility. A more comprehensive hyperelastic model, such as the Mooney-Rivlin model, would require the fitting of additional phenomenological parameters beyond the scope of the swollen polymer network model [22]. However, neither the swollen polymer network model nor the neo-Hookean model explicitly addresses the scope of its application: what are the relevant ranges for strain and time scale, and does it matter whether the force is applied during a loading or unloading phase? Further experimental characterization in a variety of conditions is needed to evaluate whether the swollen polymer network model predictions of stiffness are substantially accurate for a broad range of hydrogel formulations.

Given the assumptions related to the neo-Hookean shear modulus and rubberlike elasticity theory, there are numerous methods for measuring the stiffness of a hydrogel. Uniaxial tensile [23–26] and compressive [25,27–31] experiments apply force to a hydrogel sample in a single direction, yielding force and displacement data that can be directly analyzed using the neo-Hookean model. Parallel plate shear rheology experiments [32–36], frequently used in studies of hydrogel viscoelasticity, can also be applied to effectively elastic gels, wherein the storage modulus response to radial strain is often treated as a stand-in for the shear modulus [5,32,35,37]. Indentation experiments probe the stiffness of only a small region of a hydrogel sample, but repeated and distributed experiments can confirm the homogeneity of a sample [38]. Here, we distinguish between macroindentation [39–42] and nanoindentation [38,43–45] because the bulk stiffness of a hydrogel and the local surface stiffness measured via nanoindentation may differ. For cell migration, which depends on the local traction forces with deformations on the order of micrometers [6], local surface stiffness may be more relevant than large-scale bulk mechanics. Strikingly, prior literature on the stiffness of hydrogels does not provide robust comparisons on the advantages and disadvantages of the different stiffness characterization methods, and most reports of hydrogel stiffness only evaluate results from a single characterization method. Two notable exceptions in the literature use multi-method comparisons to validate pipette aspiration as a method of stiffness measurement for hydrogels [46,47]. Buffington et al., compared the stiffness of three polyacrylamide hydrogels with different crosslinking ratios using pipette aspiration, nanoindentation, and compression [47], and Gandin et al. compared six polyacrylamide hydrogel formulations (with non-systematic changes in polymer concentration and crosslinking ratio) using atomic force microscopy, pipette aspiration, macroindentation, rheology, and compression studies [46]. Both studies describe an interest in demonstrating the value of the pipette aspiration method. In contrast, this study aims to provide a balanced cross-evaluation of how the different commonly used hydrogel stiffness characterization techniques affect the measured stiffness for a range of hydrogel formulations with varying stiffnesses (Fig. 1).

Here, we characterize the stiffnesses of eighteen structurally varied poly(vinyl alcohol) hydrogel formulations using five common methods: tensile and compressive testing, rheology, and macro- and nanoindentation. We cross-evaluate the accuracy, precision, and relevant complementary features of each method, including measurement of Poisson's ratio, viscoelasticity, and surface-to-surface heterogeneity for each formulation as validations of the neo-Hookean modeling approach. Finally, we compare measured stiffnesses to structural predictions made with the swollen polymer network model to provide robust experimental feedback to the fundamentally derived model and to identify and address weaknesses with applying the model to real hydrogels.

2. Experimental section

2.1. Poly(Vinyl alcohol) hydrogel synthesis and swelling characterization

Poly(vinyl alcohol) (PVA) hydrogels were synthesized as previously described [21,48]. Briefly, PVA (M_n = 33,884 g/mol, PDI = 1.81;

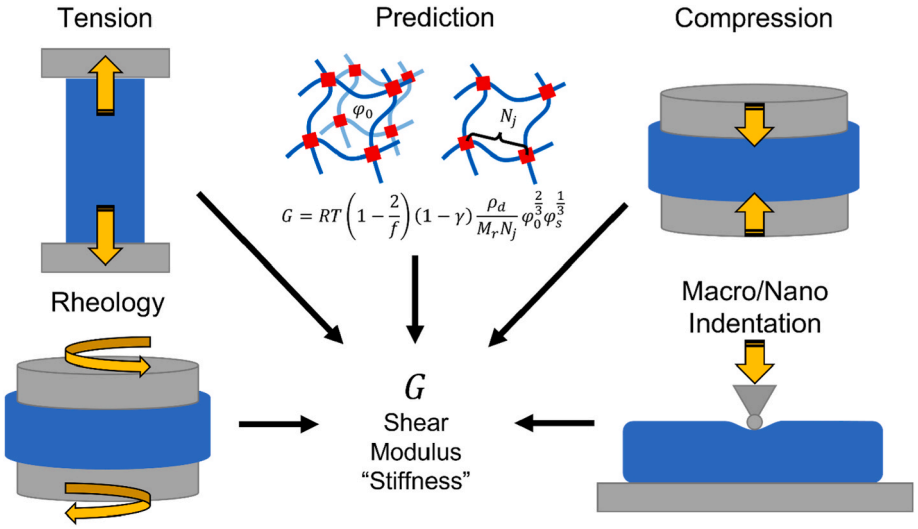

Fig. 1. Schematic comparison of stiffness measurement methods (tension, compression, rheology, macroindentation, nanoindentation) and structure-based prediction of shear modulus for hydrogels. Each approach includes distinct challenges and uncertainty, and their comparison generates a robust picture of what is understood about the mechanics of hydrogels.

Sigma-Aldrich, St. Louis, MO) was dissolved in deionized water by heating at 90 °C overnight at three concentrations corresponding to three initial polymer volume fractions (φ_0) of 5, 7.5, and 10%. PVA solutions were adjusted to ~1.5 pH with hydrochloric acid, then an aqueous glutaraldehyde solution (25%; Sigma-Aldrich) was added based on stoichiometric ratios with PVA (mol glutaraldehyde/mol PVA-repeating units) to attain six ideal degrees of polymerization between junctions (N_j) of 20, 30, 40, 50, 60, and 70. The resulting 18 combinations of initial polymer volume fractions and degrees of polymerization values were cast into ~2 mm-thick sheets and left to react for 3 h to form hydrogels. Two batches were synthesized for each formulation to address batch-to-batch variability. Following the hydrogel formation reaction, three 18 mm-diameter discs (per formulation and batch) were punched for swelling analysis, and the remaining material was swollen to equilibrium in phosphate-buffered saline (PBS) for use in mechanical experiments. Due to the dissolution at high temperature and maintaining sample hydration for the entire study, the likelihood and structural effects of PVA's tendency to crystallize in dry conditions were minimized.

As previously described [21,48], swelling was characterized in three states: the relaxed state immediately followed gelation, the swollen state followed swelling to equilibrium in excess PBS, and the dry state followed desalting in deionized water and drying with heat and vacuum. Volumes in each state were measured using a buoyancy-based method [21]. Swollen polymer volume fractions (φ_s) were calculated by dividing the swollen volume by the dry volume.

2.2. Tensile experiments and analysis

Tensile experiments were performed using a Univert tester (CellScale, Waterloo, ON) with a water bath, attached camera for digital image correlation (DIC), and custom-made shoulder-supported grips for soft hydrogel samples. Dog-bone-shaped hydrogel samples were punched from films with a custom-made punch (adapted from a previously published design [49]), yielding hydrogel samples for tensile testing with a 30 × 10 mm gage area and thicknesses ranging from 1.5 to 2.5 mm based on hydrogel swelling. Further information about the custom dog-bone punch and associated shoulder-supported grips is provided in the supplementary material.

For each of the eighteen hydrogel formulations and two batches per formulation, three dog-bone samples were punched for tensile testing ($n = 6$). The thickness of each sample was measured for later use in calculating stress. The camera-facing side of each sample was speckled with graphite to facilitate digital image correlation (DIC). Each sample was loaded into the tester and fully submerged in phosphate-buffered saline (PBS), then subject to two cycles of uniaxial extension of 6 mm at a rate of 1/3 mm per second. The applied force was measured by a 2 N load cell between the displacement arm and the sample grips. During the loading cycles, a camera attached to the tensile tester recorded video and correlated each image frame to the force applied at the time. During experimentation, the stiffest hydrogel formulation ($\varphi_0 = 0.100$, $N_j = 20$) would consistently fracture and was not included in the final analysis.

Following the tensile experiments, the UniVert DIC software was used to calculate local strain values within the homogeneous deformation region of the sample gauge area based on changes to the graphite speckle patterns. DIC-based stretching data in the x and y directions (parallel and perpendicular to the applied force) were used to calculate the Poisson's ratio of each sample [50]. By solving the homogeneous uniaxial tension boundary value problem and assuming incompressible, neo-Hookean material behavior force and y-stretch measurements were correlated (Equation (1)). Through fitting the experimental data to Equation (1), the shear modulus was identified. A link to the R script used to analyze the entire tensile dataset is provided in the supplementary material.

$$\sigma = G\left(\lambda^2 - \frac{1}{\lambda}\right) \tag{1}$$

In Equation (1), σ is the Cauchy stress based on the applied force and time-dependent cross-sectional area, G is the shear modulus, and λ is the local strain in the homogeneous deformation region.

2.3. Compressive experiments and analysis

Compressive experiments, and all mechanical experiments other than the tensile experiments, use the same set of 10 mm-diameter discs punched from the original hydrogel films. Three samples from two batches per formulation were tested ($n = 6$). Unlike with tensile testing, all samples retained their integrity through compression, rheology, macroindentation, and nanoindentation experiments, including the stiffness hydrogel formulation ($\varphi_0 = 0.100$, $N_j = 20$).

Compressive experiments were performed using a Q800 Dynamic Mechanical Analyzer (DMA; TA Instruments, New Castle, DE) equipped with compression and submerged compression clamp sets. For submersion experiments, samples were fully submerged in PBS. For non-submerged experiments, samples were preloaded to 0.01 N compressive force and then treated to two cycles of compression to 20% strain at a rate of 20% strain per minute. Submerged experiments used 0.03 N preload to overcome buoyancy effects and the same 20% strain cycles.

Following compressive experiments, raw force and length over time data were collected as text files and batch-analyzed using a custom R script (provided in supplementary material) to calculate shear modulus from the uniaxial neo-Hookean model (Equation (1)). For this analysis, compressive data was subset down to the upper half of the first loading curve (10–20% strain; see (Supp.Fig. S3) to minimize variable nonlinearity in the initial stress-strain curves, which may have resulted from non-flat sample surfaces or other imperfections in initial sample-instrument contact.

2.4. Rheological experiments and analysis

Rheological experiments were performed using a Discovery Hybrid Rheometer (TA Instruments, New Castle, DE) equipped with sand-blasted parallel flat plates (10 mm upper plate diameter). Like compression experiments, rheology experiments were performed in both PBS-submerged and non-submerged conditions using a water trap. Each sample was centered between the two plates and held in place by a 0.5 ± 0.1 N axial force. Initial amplitude sweep and frequency sweep studies showed that all hydrogel formulations were within the linear viscoelastic region at a frequency of 1 Hz and over an amplitude range including 0.1–1% rheological shear strain. Treating all the hydrogels as effectively elastic due to their covalent network structure and the relatively low oscillation frequency, we treated the average storage modulus over the 0.1–1% strain range (calculated by the rheometer's software) as an equivalent estimate of shear modulus. An R script was used to organize the data from each experiment by condition and hydrogel formulation (available in supplementary material).

2.5. Macroindentation experiments and analysis

Macroindentation experiments were performed using the Q800 DMA (TA Instruments, New Castle, DE) with a 3 mm-diameter spherical indentation probe. Each sample was preloaded to 0.01 N and then indented to 10% local strain (the tip was indented to 10% of the thickness of the sample) at 20% strain per minute. Sample thicknesses varied based on the extent of swelling to equilibrium, from 1.4 to 2.5 mm. The resulting force-displacement data from the loading phase was fit to a Hertz model (Equation (2)), and results were grouped by hydrogel formulation using an R script (supplementary material).

$$F = G\left(\frac{8r^{\frac{1}{2}}d^{\frac{3}{2}}}{3(1-\nu)}\right) \quad (2)$$

In Equation (2), F is the applied force, r is the radius of the spherical probe, d is the distance indented into the material, and ν is Poisson's ratio, assumed to be 0.5.

2.6. Nanoindentation and analysis

Nanoindentation experiments were performed using a Piuma nanoindenter (Optics11 Life, Amsterdam, Netherlands) with a 24 μm-radius probe tip and a cantilever stiffness of 0.24 N/m. For all experiments, samples were submerged in PBS, and force spectroscopy curves were measured in a square 3 × 3 grid with 50 μm raster steps. For all samples, the probe was indented up to 3 μm into the sample over 0.6 s (the total penetration depth is less than 3 μm due to force-dependent probe deflection). Because nanoindentation is more sensitive to surface stiffness than bulk stiffness when compared to other methods, nanoindentation experiments were performed on both sides of each sample to measure absolute differences in surface stiffnesses. The Piuma software fitted each force spectroscopy loading curve to a Hertz model (Equation (2)), and an R script (supplementary material) was used to calculate average values per hydrogel formulation.

2.7. Predictive structural modeling

Hydrogel swelling and stiffness were predictively modeled from the expected structure for each hydrogel formulation according to the swollen polymer network model [12,21,51]. Briefly, the swollen polymer volume fraction (φ_s) was predicted using the equilibrium swelling equation (Equation (3)) using the relevant initial polymer volume fraction (φ_0) and degree of polymerization between junctions (N_j) for each hydrogel formulation and relevant identity parameters. The predicted swollen polymer volume fraction was then used in the rubberlike elasticity equation (Equation (4)) to predict shear moduli (G) for each hydrogel formulation. Notably, this approach differs from our previously published work [21], which predicted hydrogel stiffness from swelling measurements. Here, both swelling and stiffness are predicted *a priori* from structural and identity parameters, resulting in a more fundamental prediction that does not require an intermediate measurement.

$$\varphi_s^{-\frac{1}{3}}\left[\ln(1-\varphi_s)+\varphi_s+\chi_1\varphi_s^2\right] = -1*\frac{\rho_d V_1}{M_r N_j}(1-\gamma)\left(1-\frac{2}{f}\right)\varphi_0^{\frac{2}{3}} \quad (3)$$

$$G = RT\left(1-\frac{2}{f}\right)(1-\gamma)\frac{\rho_d}{M_r N_j}\varphi_0^{\frac{2}{3}}\varphi_s^{\frac{1}{3}} \quad (4)$$

In Equation (3), $\chi_1 = 0.494$ is the polymer-solvent interaction parameter for PVA, $\rho_d = 1.27\ g/mL$ is the polymer dry density, $V_1 = 18\ mL/mol$ is the molar volume of the solvent (water), $M_r = 44\ g/\ mol$ is the repeating unit molecular weight, $f = 4$ is the junction functionality, and γ is the frequency of chain-end defects, which is calculated as $\gamma = \frac{fM_r N_j}{(f-2)M_n}$ according to Ref. [12]. $M_n = 33,884\ g/mol$ is the linear PVA molecular weight [21].

In Equation (4), $R = 8314\ J/kmol{\cdot}K$ is the ideal gas constant, and $T = 298\ K$ is the temperature.

2.8. Statistical analysis

All experiments were performed in triplicate with two batches per formulation ($n = 6$). All values are represented as mean ± standard deviation. Analysis and modeling were performed using Excel (Microsoft Corporation, Albuquerque, NM), R & RStudio scripts, GraphPad Prism 9 software (GraphPad Software, San Diego, CA), and software from mechanical testing instrument manufacturers as noted in the methods above. Quantitative (raw and processed) data for this work are available via the supplementary material.

3. Results and discussion

3.1. PVA hydrogel synthesis and swelling

Eighteen PVA hydrogel formulations were synthesized with varying initial polymer volume fractions ($\varphi_0 = 0.050,\ 0.075,\ or\ 0.100$) and degrees of polymerization between junctions ($N_j = 20,\ 30,\ 40,\ 50,\ 60,\ or\ 70$) as previously reported [21]. Each hydrogel formulation was synthesized in two batches to account for batch-to-batch variations, except for the stiffest formulation ($\varphi_0 = 0.100$, $N_j = 20$), which failed to form intact, homogeneous hydrogels in one of the batches. Three samples from each formulation and batch were used to determine the swollen polymer volume fraction (φ_s) for each formulation, which was used in a later analysis comparing model predictions to measured stiffnesses. The remaining equilibrium-swollen hydrogel material was used for stiffness measurements.

3.2. Cross-evaluation of hydrogel stiffness measurement methods

The primary goal of this work was to evaluate whether the most-used stiffness characterization methods for hydrogels reliably yielded equivalent results. To address this goal, we characterized the stiffness of eighteen PVA hydrogel formulations using tension, compression, rheology, macroindentation, and nanoindentation. Structurally varied PVA hydrogel formulations were used in this study to create chemically equivalent hydrogels that range over more than an order of magnitude in shear modulus values. While each stiffness characterization method has innate advantages and unique features that will be discussed in the next major section, they have all been used to measure shear modulus [24,31,32,42,43], which may be thought of as a universal parameter for the stiffness of a hyperelastic material. Therefore, we first compared the shear moduli as a function of the measurement method for each hydrogel formulation (Fig. 2) to identify the most accurate and precise correlations between methods.

In Fig. 2, all axes are represented on a logarithmic scale to equally represent the distribution of stiffnesses for the eighteen hydrogel formulations, which would otherwise skew toward lower stiffnesses and obscure their differences on a linear scale. The logarithmic scale also serves to balance the importance of normalized accuracy at low shear modulus values with accuracy at higher shear modulus values, especially since many hydrogel applications require materials on the softer side of the represented spectrum.

Cross-evaluation between comparable methods as shown in Fig. 2 yields two major analysis categories: accuracy and precision. Two methods with an accurate relationship have similar values over the entire range of interest and do not show significant biases away from the 1:1 correlation as shown for tension and macroindentation (Fig. 2A). Two methods with a precise relationship are highly correlated, but that correlation does not have to have equivalent values, as shown by the high R^2 value for the tension-compression relationship, despite the visible deviance from a 1:1 correlation at low stiffness (Fig. 2B). The compression-nanoindentation relationship (Fig. 2G) demonstrates a relatively accurate relationship with low precision, and the tension-rheology relationship demonstrates a relatively precise relationship ($R^2 = .9304$) with poor accuracy. The relative importance of accuracy and precision depends on the application—whether it is more important for agreement between measurement methods (accuracy) or to confirm the differences between hydrogel formulations (precision).

To assess the cross-evaluations based on individual methods, tension experiments yielded the most reliable measurements and nanoindentation yielded the least reliable measurements. The differences can partially be attributed to scale and methodology. While compression,

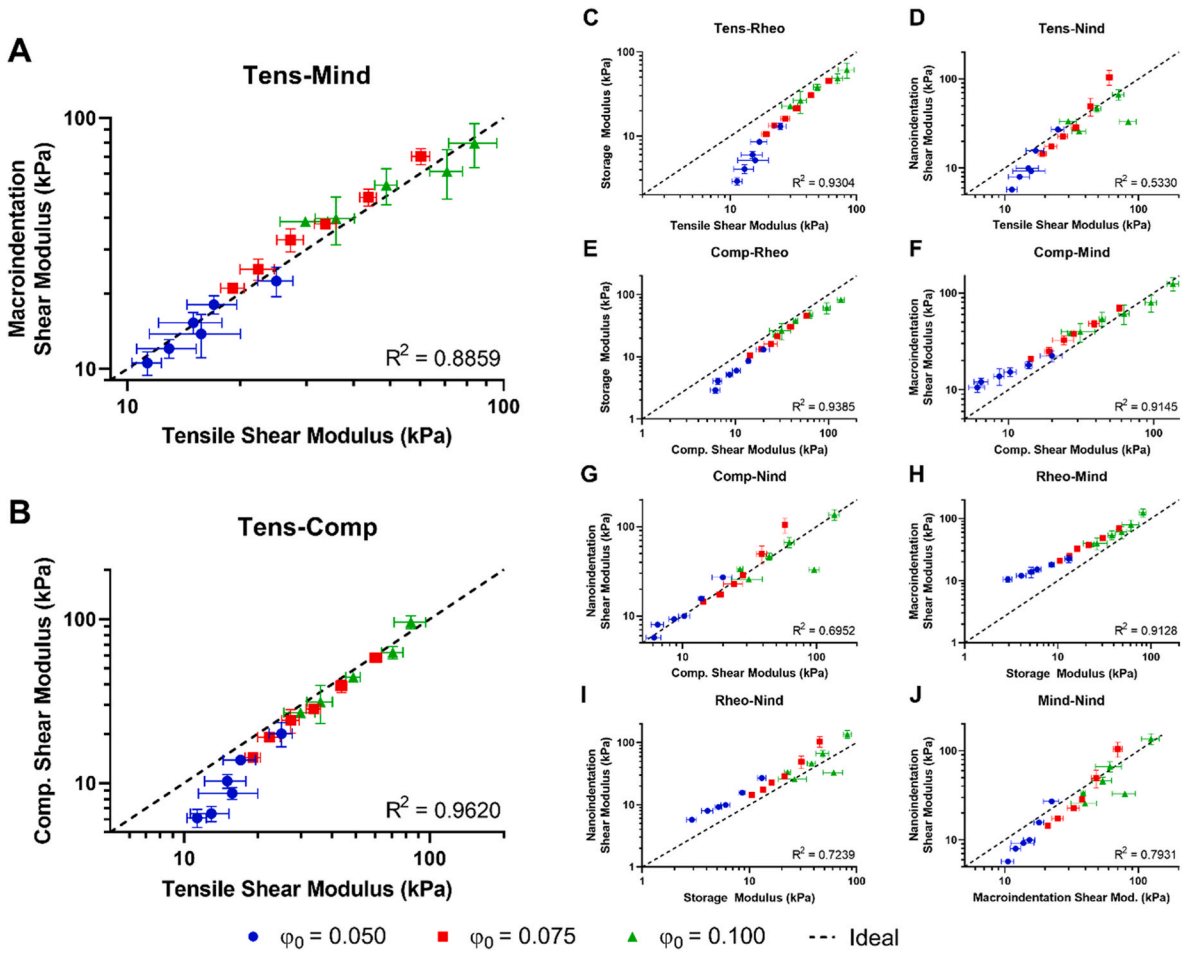

Fig. 2. Cross-evaluation of five stiffness characterization methods on eighteen structurally varied PVA hydrogels. The dotted line represents an ideal 1:1 correlation, and error bars represent standard deviations. R^2 values represent the precision of the global best fit line between the *x*-axis and *y*-axis values (best-fit line not shown). Tens: Tension. Mind: Macroindentation. Comp: Compression. Rheo: Rheology. Nind: Nanoindentation. φ_0: Initial polymer volume fraction.

rheology, and macroindentation effectively probed the stiffness of 10 mm hydrogel discs, tensile experiments analyzed a larger dogbone-shaped sample of each hydrogel formulation, and nanoindentation effectively probed only a small depth into the surface of a hydrogel sample. These results imply that, when viable, larger hydrogel samples and methods that make use of more of the sample will yield more reliable results. Furthermore, the tension experiments included DIC, creating local strain analysis that exceeded what is possible with the other methods. Direct comparison between DIC-based shear moduli measurements and overall displacement-based shear moduli for tension experiments consistently yielded a two-fold difference (Supp.Fig. S1). Therefore, if the tension experiments did not use DIC, the resulting shear moduli would differ greatly from other measurement methods, nullifying its enhanced accuracy. Conversely, the nanoindentation method used here depends on the parameters of a pre-calibrated probe and includes assumptions about how the bending of the probe's cantilever corresponds to the material's stiffness. The uncertainty associated with such an assumption-dependent method likely contributes to the relatively low precision and accuracy seen when comparing nanoindentation to other methods. Finally, the datasets for tension and nanoindentation each have limitations that may have created artifacts for overall comparison. For the tension experiments, the stiffest hydrogel formulation ($\varphi_0 = 0.100$, $N_j = 20$) was too brittle to test using the same methods as the other formulations and was not included in the final analysis, possibly distorting the analysis compared to other methods that included the stiffest formulation in their analysis and comparisons. For the nanoindentation experiments, only the second batch of hydrogels was included in the final analysis because the probe tip broke during the characterization of the first batch, and the use of a second probe might have introduced additional experimental uncertainty. The limited dataset likely enhanced the variability associated with nanoindentation experiments despite the averaging of multiple scans per sample.

The comparison of macroindentation and nanoindentation shear moduli addresses a key question of this study—whether hydrogel stiffnesses differ depending on the length scales. Both macroindentation and nanoindentation experiments were fit to a Hertzian indentation model but with different probe sizes (3 mm vs. 48 μm diameter) and measurement equipment. The resulting correlation (Fig. 2J) is positive across all formulations with some overlap of the 1:1 correlation line and the highest R^2 value among the nanoindentation comparisons (R^2 = .7931), suggesting that the overall difference between shear moduli over approximately two orders of magnitude for probe size is negligible despite the differences in the measurement methods. This result may be specific to covalently crosslinked PVA hydrogels since that is all that is studied here, but it provides evidence that length scale does not drastically alter stiffness measurements in hydrogels. Secondarily, correlations between the two indentation methods and the other stiffness measurement methods contribute toward the validation of the Hertz model applied to hydrogels.

3.3. *Method-specific features beyond measuring stiffness*

While the five measurement methods compared in this study are all

used to study hydrogel stiffness, they each provide additional capabilities and include practical limitations specific to the method. The two most relevant capabilities to the neo-Hookean interpretation of shear modulus as stiffness for hydrogels are how tensile testing with DIC can measure Poisson's ratio and how rheology can measure viscoelasticity (Fig. 3). These measurements validate the neo-Hookean assumptions that the hydrogels are incompressible and fully elastic. These and other capabilities and major limitations for each method are discussed below.

As discussed above, tensile testing with DIC is an accurate method for measuring hydrogel stiffness [52]. R^2 values for the fit of stress and stretch to the neo-Hookean model for each tensile experiment vary from 0.918 to 0.999 with a median of 0.997, suggesting an accurate fit relationship. Notably, the low-friction surfaces of hydrogels are likely to slip from clamps under tensile forces [49]. To address this slipping tendency, we 1) used shoulder-supported clamps [49] with a custom dog-bone sample shape to provide normal forces as well as friction forces holding the sample in place and 2) used DIC to measure local strain within the gauge region of the hydrogel, which is more accurate than total displacement, especially with potential sample slippage. Because DIC optically records strain, it provides the secondary function of measuring Poisson's ratio during stretching from the ratio of the parallel and perpendicular stretches [50]. For all hydrogel formulations, the measured Poisson's ratios were within one standard deviation of 0.5 (Fig. 3A), suggesting that the hydrogels were all effectively incompressible materials over the timescale of the tensile experiments (18 s, rate of 0.33 mm/s). The measured Poisson's ratios validate the incompressibility assumption of the neo-Hookean hyperelastic model applied to the studied hydrogels.

Key limitations for the tension experiment compared to the other stiffness measurement methods include the equipment requirements, the amount of sample material needed, and the time needed to optimize the experiment. For tension experiments with DIC, equipment included a tensile tester, a connected camera and lighting rig, and a computer with proprietary software needed to analyze the raw DIC data. Open-access alternatives may reduce this limitation [53]. The samples needed were larger than for the other methods because DIC required a large gauge area with an unobstructed view for high-quality analysis and the dogbone shape was necessary for shoulder-supported tension experiments. Ultimately, developing the shoulder-supporting clamps, optimizing data acquisition with the camera, and fully submerging samples in a large PBS bath during experiments caused the total experimental time commitment for this method to greatly exceed the time spent on the other methods. Additionally, the data volume per experiment for DIC-based tensile experiments greatly exceeded the other methods due to the need for high-speed, high-resolution imaging.

Compression experiments complemented tension experiments as a second uniaxial measurement method that uses the simplest form of the neo-Hookean model (Equation (1)). R^2 values for the fit of stress and stretch to the neo-Hookean model for each compression experiment vary from 0.98605 to 0.99999 with a median of 0.99966, suggesting an exceptionally accurate fit relationship. Compression experiments with a dynamic mechanical analyzer were performed with and without PBS submersion, yielding negligible differences in measured shear moduli (Supp.Fig. S2). For a typical stress-strain graph for a compression experiment (Supp.Fig. S3A), hysteresis was observed between loading and unloading phases, possibly associated with the selected strain rate, but no plastic deformation was observed, further validating a hyperelastic approach to characterizing stiffness in these hydrogels. However, the stress-strain slope often changed significantly from the initial loading to a more linear response at the higher end of the 20% strain applied, so compressive shear modulus measurements were calculated from the linear, 10–20% loading phase of the stress-strain chart for all hydrogel formulations (Supp.Fig. S3B). Overall, compression experiments made convenient, non-destructive use of 10-mm diameter disc samples and rapidly tested the relationship between uniaxial stress and strain for each hydrogel formulation.

Shear rheology experiments introduce complexity into the measurement of stiffness by addressing explicit time-dependent viscoelastic considerations. To create comparable conditions to other stiffness measurement methods, we performed parallel plate rheological experiments at an angular frequency of 1 Hz and measured storage moduli over a rheological shear strain range from 0.1 to 1%, which was found to be within the linear viscoelastic range for all hydrogel formulations studied. Critically, under these conditions, all hydrogel formulations showed viscoelastic fractions less than 2%, indicating that the hydrogels were effectively elastic (Fig. 3B). This validation step further confirms the applicability of the neo-Hookean hyperelastic model, which assumes negligible viscous or viscoelastic behavior of the material within the timescales of interest. Like the compression experiments, rheology experiments were performed in both wet (PBS) and dry environments, yielding negligible differences in the measured storage moduli (Supp. Fig. S4A). We note that the axial force applied during a rheology experiment is a potential source of experimental artifacts—at 0.1 N axial force, an apparent maximum stiffness was observed among the hydrogel formulations that was corrected when all samples were reanalyzed with 0.5 N axial force (Supp.Fig. S4B). Altogether, rheology studies provide critical investigations of the time-dependent behavior of hydrogel deformations, but their measurements of hydrogel stiffness are less accurate and straightforward than typical uniaxial stiffness measurement techniques such as tension and compression experiments.

Macroindentation and nanoindentation use spherical probes to investigate stiffness near the surface of a material. Indentation distinctly addresses size-dependent properties of a material's stiffness, unlike the other three methods, which address the bulk stiffness of a

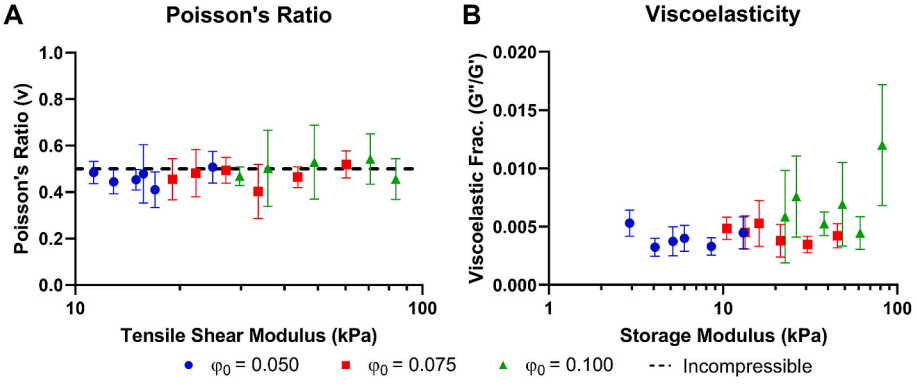

Fig. 3. Poisson's ratio and viscoelastic fraction (G"/G') measurements were collected alongside stiffness measurements via the tension and rheology methods, respectively. Data are grouped by the initial polymer volume fraction (φ_0), and error bars represent standard deviation. The dashed line represents a Poisson's ratio of 0.5, which indicates an incompressible material. Viscoelastic fraction is the average loss modulus (G") divided by the average storage modulus (G') in the linear viscoelastic range, also commonly defined as tan delta.

homogeneously deformed material. Theoretically, indentation is more likely to reflect cellular interactions with a material's stiffness since cells form focal adhesion points to push and pull on their environment [6]. Most importantly, comparing macroindentation- and nanoindentation-measured stiffnesses yielded negligible differences (Fig. 2J) and, more broadly, nanoindentation-measured stiffness with the other methods (Fig. 2D, G, I) showed that nanoscale stiffness does not consistently differ from macroscale stiffness in covalently crosslinked PVA hydrogel. However, the shallow penetration depth of nanoindentation facilitated the study of the surface-to-surface heterogeneity of the hydrogel samples (Supp.Fig. S5). Because the top and bottom surfaces were not tracked during the hydrogel swelling process, surface-to-surface heterogeneity was measured using absolute differences for each sample. While the analysis based on absolute differences does not prove whether the top or bottom surface tended to be stiffer, the apparent decrease in the difference between surface stiffnesses with increasing degrees of polymerization between junctions suggests that higher concentrations of glutaraldehyde crosslinking agent created more heterogeneity in crosslinking distributions. This result from nanoindentation experiments indicates that bulk and averaged characterizations of hydrogel stiffnesses have practical limitations that may distort understanding of local interactions.

As shown by these complementary studies, each method for stiffness characterization includes advantages and limitations. Together, they create a detailed picture of the stiffness of each hydrogel and validate assumptions associated with the definition of stiffness. However, it is time-consumptive and often redundant to use each method as done here, so readers should consider which method or combination of methods is most appropriate for their goals and downstream applications based on the features and drawbacks of each method.

3.4. Relationships between hydrogel structure and stiffness

Our theoretical understanding of how a hydrogel's stiffness relates to its network structure is guided by the swollen polymer network model [12,21,51]. Here, we manipulated the structure of PVA hydrogels by altering their initial polymer volume fractions (φ_0) and degrees of polymerization between junctions (N_j) during synthesis. The effects of varying these parameters on swelling and stiffness are well-defined within the swollen polymer network model [12,21], enabling *a priori* predictions of the swollen polymer volume fraction and shear modulus for each hydrogel formulation. We compared structure-based predictions of shear moduli to the measured shear moduli both to provide context to the measured values and to evaluate how well the theoretical predictions match the measured stiffnesses of real hydrogels (Fig. 4).

For all measurement methods, the trends relating structure to stiffness generally match the prediction. Increasing the initial polymer volume fraction (φ_0) consistently increased stiffness, and increasing the degree of polymerization between junctions (N_j) consistently decreased stiffness in a broadly inverse (1/X) relationship, yielding the highest stiffnesses and greatest changes between formulations at low degrees of polymerization between junctions and high initial polymer volume fractions. However, the prediction overestimates the stiffnesses of every formulation compared to every measurement method with the largest discrepancies at low initial polymer volume fractions and low degrees of polymerization between junctions (see Supp.Fig. S6 for direct comparison). These measurement-modeling discrepancies suggest that the fundamental assumptions in the swollen polymer network model oversimplify and idealize the network structure, and a more accurate model would need to account for the heterogeneity in the network structure, especially in the case of dilute (low φ_0) but highly crosslinked (low N_j) networks where redundant and ineffectual crosslinks are most likely to occur [20,54,55]. The current swollen polymer network model does not account for a non-Gaussian skewed distribution of degrees of polymerization between junctions that is likely for highly crosslinked networks nor does it address a kinetic theory of network formation that might reflect how network imperfections may result from dilute solutions [12,56,57]. While incorporating non-Gaussian chains and network formation kinetics into the swollen polymer network would be theoretically challenging, it may be worthwhile for the accurate design of dilute but

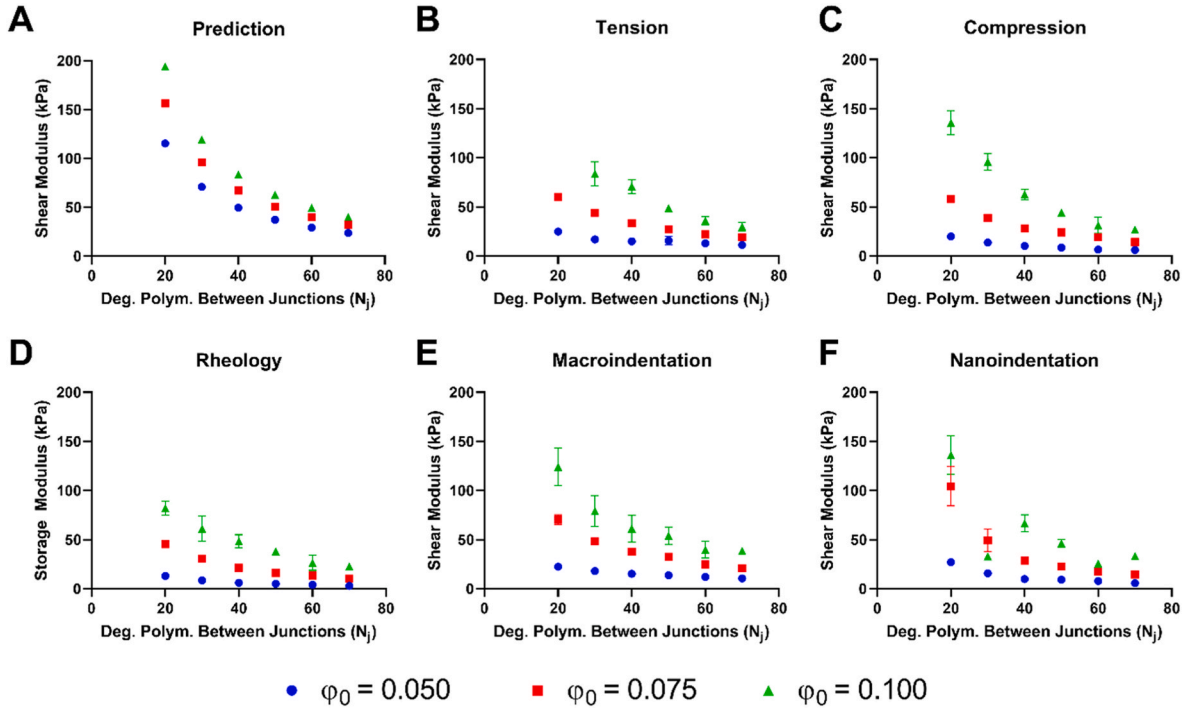

Fig. 4. Comparison of the relationship between PVA hydrogel structure and stiffness as predicted (A) and measured via five independent methods (B–F). PVA hydrogel structure is defined by the initial polymer volume fraction (φ_0) and the degree of polymerization between junctions (N_j), which were manipulated during synthesis. Error bars represent standard deviations. Predictions were made *a priori* based on the swollen polymer network model.

highly crosslinked networks that could be especially useful as size-restricting drug delivery systems.

Our prior measurements [21] of swelling in each hydrogel formulation facilitate a more nuanced analysis of the mechanisms behind the swollen polymer network model. As we have previously demonstrated, swelling measurements facilitate the prediction of a hydrogel's stiffness [21]. Here, we have used an alternative method of predicting stiffness *a priori* from the synthesis-defined network structure. With the *a priori* approach, the swollen polymer volume fraction (φ_s) is predicted first via the equilibrium swelling equation, and then the shear modulus (G) is predicted from the structural parameters and the predicted swollen polymer volume fraction via the rubberlike elasticity equation. Therefore, the swollen polymer volume fraction can be predicted or measured and the shear modulus can be predicted or measured (we are excluding shear moduli predicted from a measured swollen polymer volume fraction). The resulting comparison yields an interesting symmetry (Fig. 5): there is a universal correlation between predicted swelling and predicted stiffness (Fig. 5A) and a universal correlation between measured swelling and measured stiffness (Fig. 5B). In Fig. 5, compression-based shear moduli are used for measured stiffnesses, but the universal correlation is conserved across all measurement methods (Supp.Fig. S7). The consistency between the predicted-predicted swelling-stiffness correlation and the measured-measured swelling-stiffness correlation indicates that the predicted relationship between swollen polymer volume fraction and shear modulus, or the rubberlike elasticity equation, is appropriate. For the hydrogel formulations studied here, stiffness universally correlates with swollen polymer volume fraction. In combination with the structure-stiffness discrepancies observed in Fig. 4, these results indicate that the equilibrium swelling equation is the primary source of deviation between predicted and measured stiffness values. Furthermore, this conclusion is consistent with our previous study on hydrogel structure and swelling, which found an alternative, phenomenological relationship between hydrogel structure and swelling that was much more accurate than the predictions of the swollen polymer network (Supp.Fig. S8 shows the relationship between predicted and measured swollen polymer volume fractions) [21]. These studies provide evidence that incorrect assumptions encoded in the equilibrium swelling equation may be the limiting factor in accurately predicting the physical properties of PVA hydrogels via the swollen polymer network model.

4. Conclusions

The goals of this study were to provide a robust comparison of stiffness measurement methods for hydrogels and to investigate the fundamental relationships between hydrogel structure and stiffness. Both goals were achieved using a library of eighteen PVA hydrogel formulations varying in both the initial polymer volume fraction (φ_0) and the degree of polymerization between junctions (N_j). Tension, compression, rheology, macroindentation, and nanoindentation experiments created five independent measurements of stiffness for each hydrogel formulation, and each method provided additional answers to unique contextual questions such as the incompressibility, viscoelasticity, and heterogeneity of the hydrogels. The five stiffness measurement methods yielded broadly equivalent results. Ultimately, no one method studied here is unequivocally superior to the others, and all should be considered based on the resources available and the desired application for the hydrogel.

This study introduced a powerful, structure-based method for making *a priori* predictions of a hydrogel's stiffness. The prediction matched trends in how the variations in hydrogel structure affected measured stiffnesses, and all predicted values were within an order of magnitude of the measured values without the use of phenomenological fitting parameters. While this approach marks a significant step in quantifiable hydrogel design, it also reveals areas that can be improved. The accuracy of the model dropped at the lower ranges of initial polymer volume fraction and degree of polymerization between junctions, suggesting that the model fails to capture the effects of non-ideal network formation conditions. A closer investigation of the relationship between swelling and stiffness in this set of hydrogels suggested that the prediction errors are more closely associated with the equilibrium swelling component of the swollen polymer network model than the rubberlike elasticity component, which further confirms the importance of inconsistencies previously observed between predicted and measured synthesis-swelling relationships [21].

Further work to improve structure-based predictions of hydrogel physical properties will benefit from expanding the scope of hydrogel formulations and experimental conditions. Experimentally, PVA hydrogels were shown to follow neo-Hookean mechanics under narrow strain ranges and timescales. Most likely, the hydrogels behave more viscoelastically at higher frequencies and should even lose their incompressibility under long-term deformation by exuding water. The significance of these behaviors should be associated with the relevant applications by the Deborah number [58]. Furthermore, the idiosyncratic properties of PVA hydrogels, such as the randomness of their glutaraldehyde crosslinking reaction, may create structure-stiffness interactions that are not observed in other hydrogel systems. Equivalent studies with complementary systems, especially systems that can manipulate additional structural parameters such as junction functionality (f in Eqs. (3) and (4)) and the frequency of chain-end defects (γ in Eqs. (3) and (4)) will improve the comparisons between measured and predicted structure-property relationships and could collectively justify

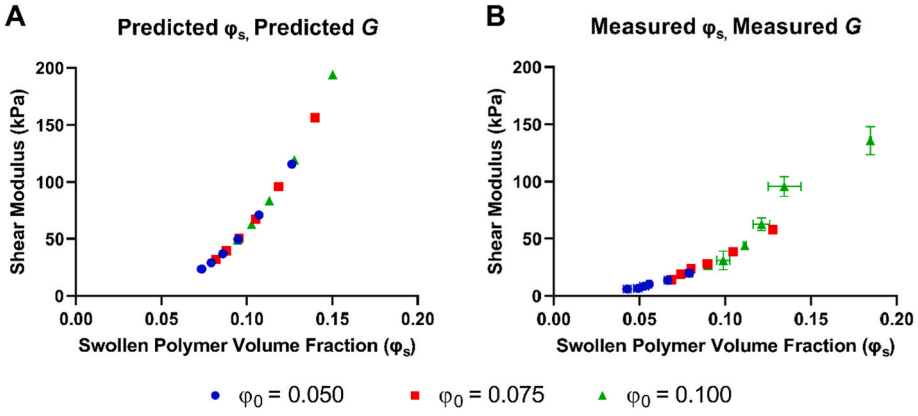

Fig. 5. Correlations between measured and model-predicted swelling and stiffness. Fully *a priori* predictions (A) show a strong swelling-stiffness correlation that is matched by the measured swelling and stiffness (B). Error bars represent standard deviations. Measured stiffness values are based on compression measurements. φ_0: initial polymer volume fraction.

changes to the fundamental models. The overarching goal of this ongoing work—to create reliable universal models for hydrogel design—will greatly accelerate biomaterials science toward translational achievements.

CRediT authorship contribution statement

Nathan R. Richbourg: Conceptualization, Methodology, Software, Validation, Formal analysis, Investigation, Data curation, Writing – original draft, Writing – review & editing, Visualization. **Manuel K. Rausch:** Conceptualization, Resources, Writing – review & editing, Supervision, Funding acquisition. **Nicholas A. Peppas:** Conceptualization, Resources, Writing – review & editing, Funding acquisition.

Declaration of competing interest

The authors declare that they have no known competing financial interests or personal relationships that could have appeared to influence the work reported in this paper.

Data availability

I have shared the link to the data in the supplementary materials.

Acknowledgments

The authors would like to acknowledge Dr. Will Meador, Gabriella Sugerman, and Sebastian Salvador for their assistance with tensile experiments. Support for this work was provided by the National Science Foundation (1610403 for N.R.R. and 2046148, 2105175, and 1916663 for M.K.R.) and the National Institutes of Health (EB022025, GM043337 for N.A.P.). N.A.P. is further supported by the Cockrell Family Regents Chair in Engineering for the Institute of Biomaterials, Drug Delivery, and Regenerative Medicine and the UT-Portugal Collaborative Research Program. N.R.R. is further supported by the Cockrell Graduate Continuing Fellowship.

Appendix A. Supplementary data

Supplementary data to this article can be found online at https://doi.org/10.1016/j.polymer.2022.125316.

References

[1] S.R. Caliari, J.A. Burdick, A practical guide to hydrogels for cell culture, Nat. Methods 13 (2016) 405–414.
[2] M.E. Wechsler, R.E. Stephenson, A.C. Murphy, H.F. Oldenkamp, A. Singh, N. A. Peppas, Engineered microscale hydrogels for drug delivery, cell therapy, and sequencing, Biomed. Microdevices 21 (2) (2019) 31.
[3] S.O. Blacklow, J. Li, B.R. Freedman, M. Zeidi, C. Chen, D.J. Mooney, Bioinspired mechanically active adhesive dressings to accelerate wound closure, Sci. Adv. 5 (7) (2019), eaaw3963.
[4] S. Correa, A.K. Grosskopf, H. Lopez Hernandez, D. Chan, A.C. Yu, L.M. Stapleton, E. A. Appel, Translational applications of hydrogels, Chem. Rev. 121 (18) (2021) 11385–11457.
[5] K.A. Kyburz, K.S. Anseth, Three-dimensional hMSC motility within peptide-functionalized PEG-based hydrogels of varying adhesivity and crosslinking density, Acta Biomater. 9 (5) (2013) 6381–6392.
[6] K. Adebowale, Z. Gong, J.C. Hou, K.M. Wisdom, D. Garbett, H.-p. Lee, S. Nam, T. Meyer, D.J. Odde, V.B. Shenoy, O. Chaudhuri, Enhanced substrate stress relaxation promotes filopodia-mediated cell migration, Nat. Mater. 20 (2021) 1290–1299.
[7] A.J. Engler, S. Sen, H.L. Sweeney, D.E. Discher, Matrix elasticity directs stem cell lineage specification, Cell 126 (4) (2006) 677–689.
[8] D.E. Discher, P. Janmey, W. Yu-li, Tissue cells feel and respond to the stiffness of their substrate, Science 310 (5751) (2005) 1139–1143.
[9] J. Prager, C.F. Adams, A.M. Delaney, G. Chanoit, J.F. Tarlton, L.-F. Wong, D. M. Chari, N. Granger, Stiffness-matched biomaterial implants for cell delivery: clinical, intraoperative ultrasound elastography provides a 'target' stiffness for hydrogel synthesis in spinal cord injury, J. Tissue Eng. 11 (2020), 2041731420934806.
[10] C.M. Tringides, N. Vachicouras, I. de Lázaro, H. Wang, A. Trouillet, B.R. Seo, A. Elosegui-Artola, F. Fallegger, Y. Shin, C. Casiraghi, K. Kostarelos, S.P. Lacour, D. J. Mooney, Viscoelastic surface electrode arrays to interface with viscoelastic tissues, Nat. Nanotechnol. 16 (9) (2021) 1019–1029.
[11] W.K. Wan, G. Campbell, Z.F. Zhang, A.J. Hui, D.R. Boughner, Optimizing the tensile properties of polyvinyl alcohol hydrogel for the construction of a bioprosthetic heart valve stent, J. Biomed. Mater. Res. 63 (6) (2002) 854–861.
[12] N.R. Richbourg, N.A. Peppas, The swollen polymer network hypothesis: quantitative models of hydrogel swelling, stiffness, and solute transport, Prog. Polym. Sci. 105 (2020), 101243.
[13] D.C. Lin, F. Horkay, Nanomechanics of polymer gels and biological tissues: a critical review of analytical approaches in the Hertzian regime and beyond, Soft Matter 4 (4) (2008) 669–682.
[14] K. Upadhyay, G. Subhash, D. Spearot, Thermodynamics-based stability criteria for constitutive equations of isotropic hyperelastic solids, J. Mech. Phys. Solid. 124 (2019) 115–142.
[15] A.S. Mijailovic, S. Galarza, S. Raayai-Ardakani, N.P. Birch, J.D. Schiffman, A. J. Crosby, T. Cohen, S.R. Peyton, K.J. Van Vliet, Localized characterization of brain tissue mechanical properties by needle induced cavitation rheology and volume controlled cavity expansion, J. Mech. Behav. Biomed. Mater. 114 (2021), 104168.
[16] O. Chaudhuri, J. Cooper-White, P.A. Janmey, D.J. Mooney, V.B. Shenoy, Effects of extracellular matrix viscoelasticity on cellular behaviour, Nature 584 (7822) (2020) 535–546.
[17] M.R. Islam, M.L. Oyen, A poroelastic master curve for time-dependent and multiscale mechanics of hydrogels, J. Mater. Res. 36 (2021) 2582–2590.
[18] M.L. Oyen, Nanoindentation of hydrated materials and tissues, Curr. Opin. Solid State Mater. Sci. 19 (6) (2015) 317–323.
[19] Y. Hu, J.-O. You, D.T. Auguste, Z. Suo, J.J. Vlassak, Indentation: a simple, nondestructive method for characterizing the mechanical and transport properties of pH-sensitive hydrogels, J. Mater. Res. 27 (1) (2012) 152–160.
[20] B. Erman, J.E. Mark, Structures and Properties of Rubberlike Networks, Oxford University Press, 1997.
[21] N.R. Richbourg, M. Wancura, A.E. Gilchrist, S. Toubbeh, B.A.C. Harley, E. Cosgriff-Hernandez, N.A. Peppas, Precise control of synthetic hydrogel network structure via linear, independent synthesis-swelling relationships, Sci. Adv. 7 (7) (2021), eabe3245.
[22] K. Upadhyay, G. Subhash, D. Spearot, Hyperelastic constitutive modeling of hydrogels based on primary deformation modes and validation under 3D stress states, Int. J. Eng. Sci. 154 (2020), 103314.
[23] D.P. Browe, C. Wood, M.T. Sze, K.A. White, T. Scott, R.M. Olabisi, J.W. Freeman, Characterization and optimization of actuating poly(ethylene glycol) diacrylate/acrylic acid hydrogels as artificial muscles, Polymer 117 (2017) 331–341.
[24] S. Wu, M. Hua, Y. Alsaid, Y. Du, Y. Ma, Y. Zhao, C.-Y. Lo, C. Wang, D. Wu, B. Yao, J. Strzalka, H. Zhou, X. Zhu, X. He, Poly(vinyl alcohol) hydrogels with broad-range tunable mechanical properties via the hofmeister effect, Adv. Mater. 33 (11) (2021), 2007829.
[25] K. Mitsuhashi, S. Ohta, T. Ito, Analysis of model drug permeation through highly crosslinked and biodegradable polyethylene glycol membranes, J. Membr. Sci. 645 (2022), 120218.
[26] M.W. Tibbitt, A.M. Kloxin, L.A. Sawicki, K.S. Anseth, Mechanical properties and degradation of chain and step-polymerized photodegradable hydrogels, Macromolecules 46 (7) (2013) 2785–2792.
[27] S. Pedron, A.M. Pritchard, G.A. Vincil, B. Andrade, S.C. Zimmerman, B.A.C. Harley, Patterning three-dimensional hydrogel microenvironments using hyperbranched polyglycerols for independent control of mesh size and stiffness, Biomacromolecules 18 (4) (2017) 1393–1400.
[28] S. Lee, X. Tong, F. Yang, The effects of varying poly(ethylene glycol) hydrogel crosslinking density and the crosslinking mechanism on protein accumulation in three-dimensional hydrogels, Acta Biomater. 10 (10) (2014) 4167–4174.
[29] C. Cha, J.H. Jeong, J. Shim, H. Kong, Tuning the dependency between stiffness and permeability of a cell encapsulating hydrogel with hydrophilic pendant chains, Acta Biomater. 7 (10) (2011) 3719–3728.
[30] C. Cha, S.Y. Kim, L. Cao, H. Kong, Decoupled control of stiffness and permeability with a cell-encapsulating poly(ethylene glycol) dimethacrylate hydrogel, Biomaterials 31 (18) (2010) 4864–4871.
[31] J.A. Beamish, J. Zhu, K. Kottke-Marchant, R.E. Marchant, The effects of monoacrylated poly(ethylene glycol) on the properties of poly(ethylene glycol) diacrylate hydrogels used for tissue engineering, J. Biomed. Mater. Res., Part A 92A (2) (2010) 441–450.
[32] T. Fujiyabu, Y. Yoshikawa, J. Kim, N. Sakumichi, U.-i. Chung, T. Sakai, Shear modulus dependence of the diffusion coefficient of a polymer network, Macromolecules 52 (24) (2019) 9613–9619.
[33] M.S. Rehmann, K.M. Skeens, P.M. Kharkar, E.M. Ford, E. Maverakis, K.H. Lee, A. M. Kloxin, Tuning and predicting mesh size and protein release from step growth hydrogels, Biomacromolecules 18 (10) (2017) 3131–3142.
[34] J. Kim, Y.P. Kong, S.M. Niedzielski, R.K. Singh, A.J. Putnam, A. Shikanov, Characterization of the crosslinking kinetics of multi-arm poly(ethylene glycol) hydrogels formed via Michael-type addition, Soft Matter 12 (7) (2016) 2076–2085.
[35] D. Gvaramia, E. Müller, K. Müller, P. Atallah, M. Tsurkan, U. Freudenberg, M. Bornhäuser, C. Werner, Combined influence of biophysical and biochemical cues on maintenance and proliferation of hematopoietic stem cells, Biomaterials 138 (2017) 108–117.
[36] J. Yang, Y. Li, Y. Liu, D. Li, L. Zhang, Q. Wang, Y. Xiao, X. Zhang, Influence of hydrogel network microstructures on mesenchymal stem cell chondrogenesis in vitro and in vivo, Acta Biomater. 91 (2019) 159–172.

[37] D.E. Liu, C. Kotsmar, F. Nguyen, T. Sells, N.O. Taylor, J.M. Prausnitz, C.J. Radke, Macromolecule sorption and diffusion in HEMA/MAA hydrogels, Ind. Eng. Chem. Res. 52 (50) (2013) 18109–18120.
[38] M.D.A. Norman, S.A. Ferreira, G.M. Jowett, L. Bozec, E. Gentleman, Measuring the elastic modulus of soft culture surfaces and three-dimensional hydrogels using atomic force microscopy, Nat. Protoc. 16 (5) (2021) 2418–2449.
[39] K.-i. Hoshino, T. Nakajima, T. Matsuda, T. Sakai, J.P. Gong, Network elasticity of a model hydrogel as a function of swelling ratio: from shrinking to extreme swelling states, Soft Matter 14 (47) (2018) 9693–9701.
[40] L.E. Jansen, H. Kim, C.L. Hall, T.P. McCarthy, M.J. Lee, S.R. Peyton, A Poly (ethylene Glycol) Three-Dimensional Bone Marrow Hydrogel, Biomaterials, 2021, 121270.
[41] S. Galarza, A.J. Crosby, C. Pak, S.R. Peyton, Control of astrocyte quiescence and activation in a synthetic brain hydrogel, Adv. Healthcare Mater. 9 (4) (2020), 1901419.
[42] B.S. Spearman, N.K. Agrawal, A. Rubiano, C.S. Simmons, S. Mobini, C.E. Schmidt, Tunable methacrylated hyaluronic acid-based hydrogels as scaffolds for soft tissue engineering applications, J. Biomed. Mater. Res. 108 (2) (2020) 279–291.
[43] A.E. Gilchrist, S. Lee, Y. Hu, B.A.C. Harley, Soluble signals and remodeling in a synthetic gelatin-based hematopoietic stem cell niche, Adv. Healthcare Mater. 8 (2019), 1900751, 0.
[44] D.A. Foyt, D.K. Taheem, S.A. Ferreira, M.D.A. Norman, J. Petzold, G. Jell, A. E. Grigoriadis, E. Gentleman, Hypoxia impacts human MSC response to substrate stiffness during chondrogenic differentiation, Acta Biomater. 89 (2019) 73–83.
[45] E.A. Phelps, N.O. Enemchukwu, V.F. Fiore, J.C. Sy, N. Murthy, T.A. Sulchek, T. H. Barker, A.J. García, Maleimide cross-linked bioactive PEG hydrogel exhibits improved reaction kinetics and cross-linking for cell encapsulation and in situ delivery, Adv. Mater. 24 (1) (2012) 64–70.
[46] A. Gandin, Y. Murugesan, V. Torresan, L. Ulliana, A. Citron, P. Contessotto, G. Battilana, T. Panciera, M. Ventre, A.P. Netti, L. Nicola, S. Piccolo, G. Brusatin, Simple yet effective methods to probe hydrogel stiffness for mechanobiology, Sci. Rep. 11 (1) (2021), 22668.
[47] C.M. Buffinton, K.J. Tong, R.A. Blaho, E.M. Buffinton, D.M. Ebenstein, Comparison of mechanical testing methods for biomaterials: pipette aspiration, nanoindentation, and macroscale testing, J. Mech. Behav. Biomed. Mater. 51 (2015) 367–379.
[48] N.R. Richbourg, N.A. Peppas, High-throughput FRAP analysis of solute diffusion in hydrogels, Macromolecules 54 (22) (2021) 10477–10486.
[49] P. Moy, T. Weerasooriya, C.A. Gunnarsson, Tensile deformation of ballistic gelatin as a function of loading rate, in: Proceedings of the XIth International Congress and Exposition June, 2008, pp. 2–5.
[50] R.H. Pritchard, P. Lava, D. Debruyne, E.M. Terentjev, Precise determination of the Poisson ratio in soft materials with 2D digital image correlation, Soft Matter 9 (26) (2013) 6037–6045.
[51] N.R. Richbourg, A. Ravikumar, N.A. Peppas, Solute transport dependence on 3D geometry of hydrogel networks, Macromol. Chem. Phys. 222 (16) (2021), 2100138.
[52] G. Subhash, Q. Liu, D.F. Moore, P.G. Ifju, M.A. Haile, Concentration dependence of tensile behavior in agarose gel using digital image correlation, Exp. Mech. 51 (2) (2011) 255–262.
[53] G.P. Sugerman, M.K. Rausch, Teaching material testing and characterization with an open, accessible, and affordable mechanical test device, Biomed. Eng. Educ. 2 (2021) 69–74.
[54] T.-S. Lin, R. Wang, J.A. Johnson, B.D. Olsen, Revisiting the elasticity theory for real Gaussian phantom networks, Macromolecules 52 (4) (2019) 1685–1694.
[55] M. Zhong, R. Wang, K. Kawamoto, D. Olsen Bradley, A. Johnson Jeremiah, Quantifying the impact of molecular defects on polymer network elasticity, Science 353 (6305) (2016) 1264–1268.
[56] J. Kovac, Modified Gaussian model for rubber elasticity, Macromolecules 11 (2) (1978) 362–365.
[57] K. Nishi, H. Noguchi, T. Sakai, M. Shibayama, Rubber elasticity for percolation network consisting of Gaussian chains, J. Chem. Phys. 143 (18) (2015), 184905.
[58] M.J. Webber, M.W. Tibbitt, Dynamic and reconfigurable materials from reversible network interactions, Nat. Rev. Mater. 7 (2022) 541–556.